THE ROYAL SOCIETY

J. R. Soc. Interface (2004) **1**, 3–15
DOI: 10.1098/rsif.2004.0002

Application of structural analysis to the mechanical behaviour of the cornea

Kevin Anderson, Ahmed El-Sheikh† and Timothy Newson

Division of Civil Engineering, University of Dundee, Dundee DD1 4HN, UK

Structural engineering analysis tools have been used to improve the understanding of the biomechanical behaviour of the cornea. The research is a multi-disciplinary collaboration between structural engineers, mathematical and numerical analysts, ophthalmologists and clinicians. Mathematical shell analysis and nonlinear finite-element modelling have been used in conjunction with laboratory experiments to study the behaviour of the cornea under different loading states and to provide improved predictions of the mechanical response to disease and injury. The initial study involved laboratory tests and mathematical back analysis to determine the corneal material properties and topography. These data were then used to facilitate the construction of accurate finite-element models that are able to reliably trace the performance of cornea upon exposure to disease, injury or elevated intra-ocular pressure. The models are being adapted to study the response to keratoconus (a disease causing loss of corneal tissue) and to tonometry procedures, which are used to measure the intra-ocular pressure. This paper introduces these efforts as examples of the application of structural engineering analysis tools and shows their potential in the field of corneal biomechanics.

Keywords: structural analysis; corneal biomechanics; mathematical analysis; numerical modelling

1. INTRODUCTION

The cornea performs three major functions: (a) it protects the inner contents of the eye; (b) it maintains the shape of the eye; and (c) it refracts light. Disease and injury can alter the shape and thickness of the cornea, leading to serious changes in the visual performance of the eye (Leibowitz & Waring 1998). For this reason, understanding the biomechanical response of the cornea to agents such as disease, surgery and injury is of great clinical importance. This task is made difficult by the layered structure of the cornea and its lack of homogeneity. Both factors mean that losing corneal tissue due to disease and surgery affects the cornea's material properties and makes predicting the effects of these agents more difficult.

The research presented in this paper employs engineering, mathematical and numerical techniques to model the behaviour of the cornea under external effects such as disease and surgery and internal effects such as intra-ocular pressure (IOP) change. Accuracy is achieved through incorporation of the actual material properties and topography of the cornea. Experimental testing of corneal trephinates (buttons) is conducted to determine the material properties, and the specimens were further subjected to laser scanning to determine their topography.

Mathematical analysis based on shell theory was utilized to derive the material constitutive relationship from the experimental results. The constitutive relationship found was highly nonlinear, with two distinctive phases indicating significant stiffening beyond a certain level of loading. This knowledge of the material properties and corneal topography was essential for building an accurate representative model based on finite-element techniques. This paper presents a brief account of the research undertaken and the results obtained. Reference will be given to earlier publications and future directions for the work described.

The research has concentrated on porcine corneas because of their close similarity with human corneas in structure and constitutive relationship (Zeng *et al.* 2001). This work has enabled the identification of important aspects of the material properties and the determination of the significant factors that should be considered in the numerical modelling. This step is important because of the inherent complexity of the corneal structure at both the micro and macro levels, and hence the need to simplify the model and allow it to incorporate only the significant factors. Once this step of the research is completed, the main findings will be validated for human corneas.

2. CORNEAL STRUCTURE

The cornea consists of three distinct cell layers: the outer epithelium; the inner endothelium; and the central stroma, see figure 1. Between these layers are specialized extracellular structures called Bowman's and Descemet's membranes. The constitution of the three layers varies considerably, with the endothelium

†Author for correspondence (a.i.h.elsheikh@dundee.ac.uk).

Received 1 April 2004
Accepted 28 April 2004
Published online 5 May 2004

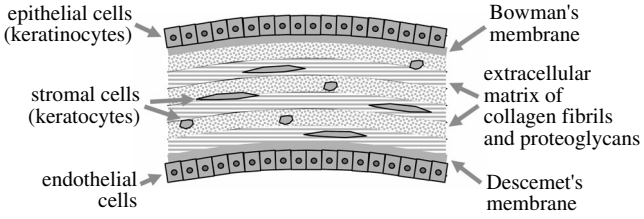

Figure 1. Cross-section through the cornea.

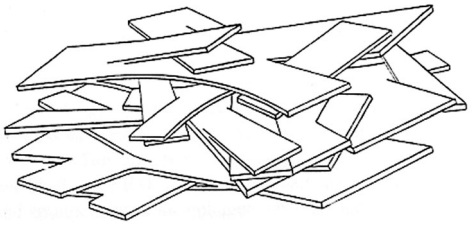

Figure 2. The interlacing of collagen lamellae in the corneal stroma.

and epithelium layers known to possess higher in-plane stiffness compared with the initial stiffness of the stroma. This variation poses the question of whether the cornea should be treated as a composite structure or as a homogeneous structure with equivalent properties. The answer to this question will undoubtedly have implications for the cost of modelling and analysis.

At the micro level, the stroma, which forms about 90% of the corneal thickness, is made up of interlacing layers of collagen fibrils embedded within a matrix of proteoglycans (Radner *et al.* 1998; Scott 1991), as depicted in figure 2. This construction not only raises questions on whether the stroma can be considered a homogeneous structure from a macro viewpoint, it also leads to difficulties in understanding the material behaviour as explained below.

3. EXPERIMENTAL TESTING

Early experimental efforts were undertaken by Woo *et al.* (1972). In their experiments whole corneas were pressure tested and the results showed a nonlinear material behaviour with significant stiffening at higher pressure levels. However, the method they used to monitor the displacement under pressure, which involved covering the corneas in ink, was thought to have affected their response to pressure. Similar tests were more recently undertaken by Bryant and McDonnell (1996) and they gave further evidence of the nonlinear nature of the corneal material. The material was observed to behave linearly to a range of IOPs between 2 and 4 kPa. Beyond this pressure, the modulus of elasticity grew suddenly. Bryant & McDonnell (1996) used a fibre optic probe and a small dot of paint (1–2 mm) on the cornea's centre to measure displacement—a method which was reported to have produced some inaccuracies in the results. The nonlinear behaviour of the cornea was also confirmed by Nyquist as early as 1968 when he investigated the biomechanical behaviour of porcine corneas using strip testing (Nyquist 1968).

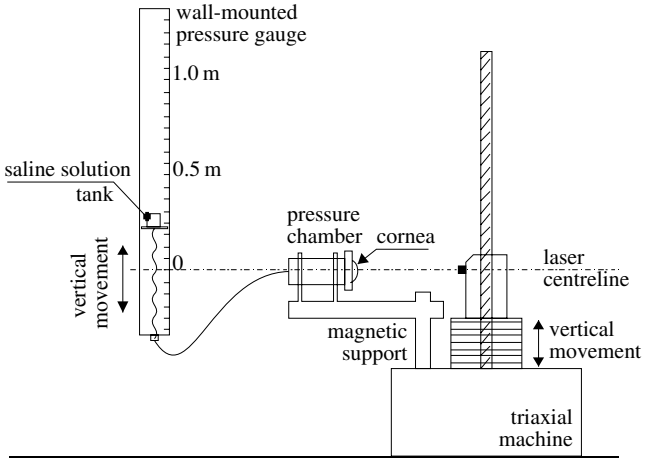

Figure 3. Trephinate inflation test rig.

In the present research, 20 porcine corneal specimens were subjected to internal pressure increases while their performance was monitored. The specimens (also called buttons or trephinates) included the cornea and a narrow ring of surrounding scleral tissue and they were no more than four hours post mortem when tested. They were mechanically separated from the rest of the eye globe using a sharp trephine cutting tool, then mounted onto a specially designed test rig that could provide watertight edge fixity for the specimens along their ring of scleral tissue. The specimens were subjected to a gradually increasing posterior pressure caused by a column of saline water to simulate the effect of elevated IOP, as shown in figure 3. In the meantime, a laser (Keyence, CCD laser displacement sensor, LK series) was used to continually monitor the displacement at the apex of the cornea. The data related to the applied pressure and the corresponding apical displacement were automatically recorded for later analysis. Care was taken to consider the natural differences in the size of the specimens and in positioning the specimens relative to the laser. To ensure a good seal along the edge of the specimens, mechanical clamps and cyano-acrylate glue were used and found to be effective. Loss of hydration was also prevented by coating the specimens in mineral oil. All corneas were subjected to a gradually increasing posterior pressure up to a maximum pressure of 14 kPa. This pressure was well above the level at which the corneas entered a stage of stable behaviour that was expected to continue until bursting.

4. EXPERIMENTAL RESULTS

The results in figure 4 show the pressure–apical rise relationships obtained for a representative selection of the trephinate inflation tests. The results show a short initial inflating stage preceding a long phase of linear behaviour, followed by sudden stiffening at about 4 kPa ($0.004\,\mathrm{N\,mm^{-2}}$). Based on the results of earlier studies by Woo *et al.* (1972) and Hjortdal (1993, 1998) on the corneal microstructure and what has been found in current laboratory testing, it is suggested that the stress–strain relationship is divided into two distinctive phases: a matrix regulated phase with low stiffness followed by

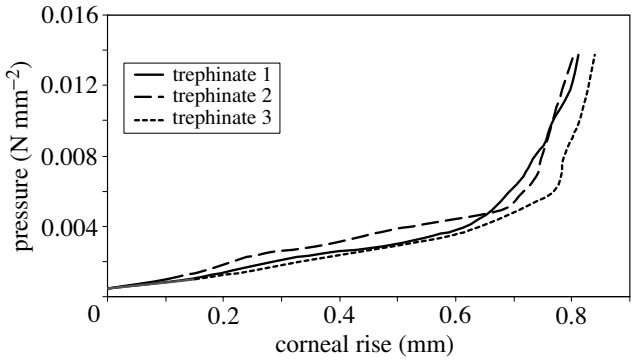

Figure 4. Pressure–apical rise experimental results.

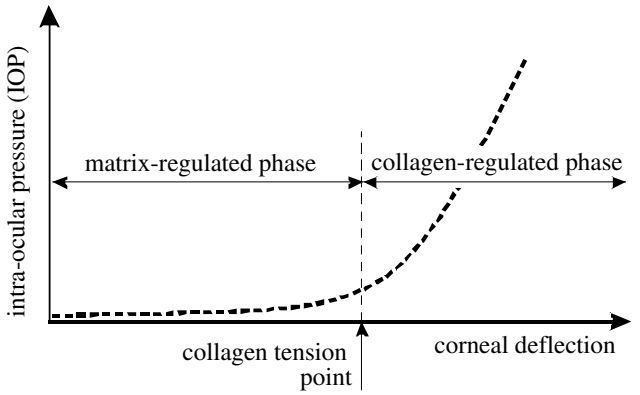

Figure 5. Corneal behaviour with an initial matrix regulated phase followed by a higher stiffness collagen regulated phase.

a collagen regulated phase with much higher stiffness, as seen in figure 5. In the first phase, the behaviour is dominated by the corneal matrix, particularly within the stroma layer. As a result, the apical rise of the cornea increases almost linearly with pressure at a low stiffness. The collagen fibril layers in this phase remain loose and unable to contribute notably to the overall performance. Then, with the start of the second phase, it is expected that the fibril layers become taut and, due to their much higher stiffness, they start to control the overall behaviour and lead quickly to a much increased corneal stiffness. Note also that these two phases of behaviour are preceded by a short phase in which the corneal specimen is initially relaxed and gradually inflated to assume its natural curved topography.

5. MATERIAL CONSTITUTIVE MODELLING

The nonlinear behaviour observed experimentally could be due to the curved profile of the cornea or due to nonlinear material properties. Mathematical analysis is used in this work to assess the effect of these factors and to develop a material constitutive relationship, which could be incorporated into the finite-element model. For simplicity, the mathematical analysis assumes that the cornea can be approximated as a homogenous (Vito *et al.* 1989) spherical structure with a constant thickness.

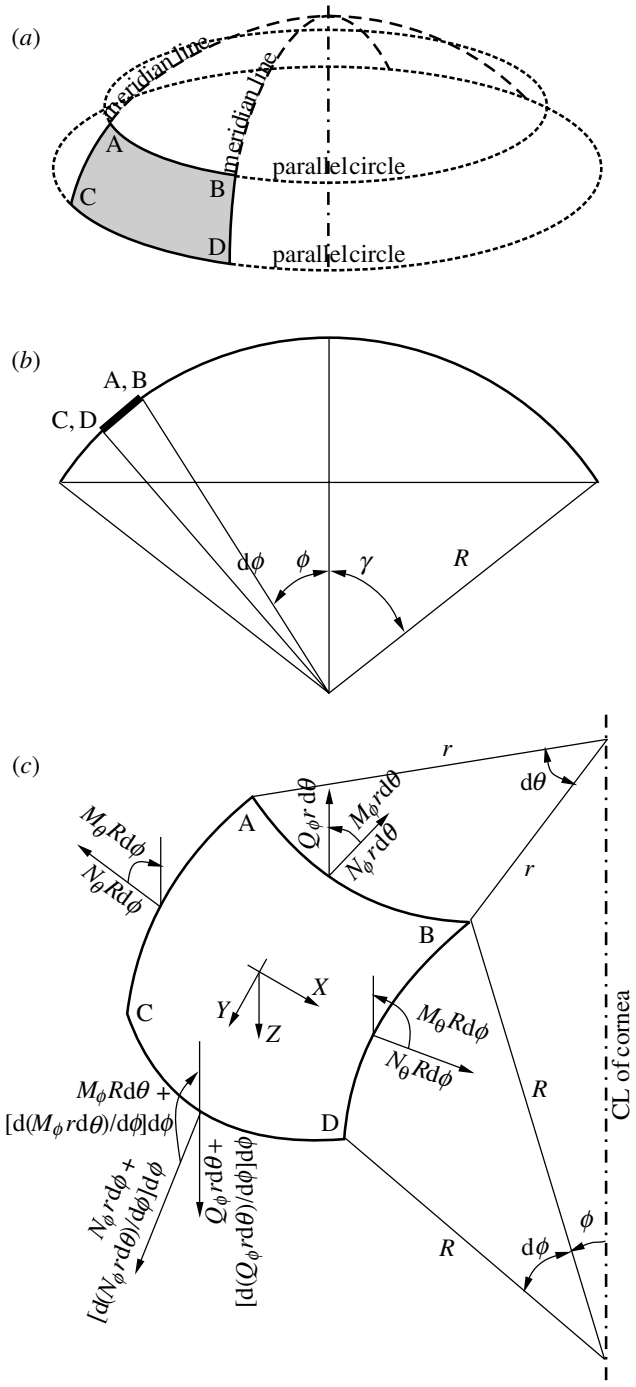

Figure 6. Mathematical analysis of corneal trephinate inflation tests: (*a*) element ABCD bounded by two meridian lines and two parallel circles; (*b*) section along a meridian line; (*c*) straining actions affecting element ABCD.

The mathematical analysis is based on shell theory and is used to study the behaviour of corneal buttons during the inflation tests. The analysis considers both in-plane and out-of-plane stiffness. It uses the pressure–apical rise data obtained experimentally in order to obtain the stress–strain relationship (or the constitutive relationship) of the material.

The analysis starts with the general spherical element bounded by two meridian lines and two parallel

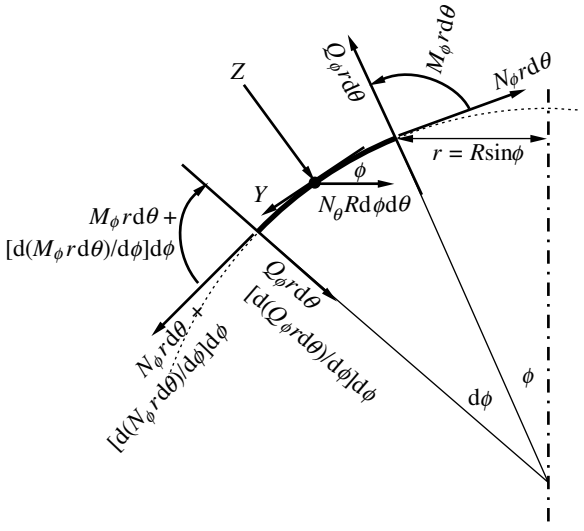

Figure 7. Straining actions acting in the meridian direction.

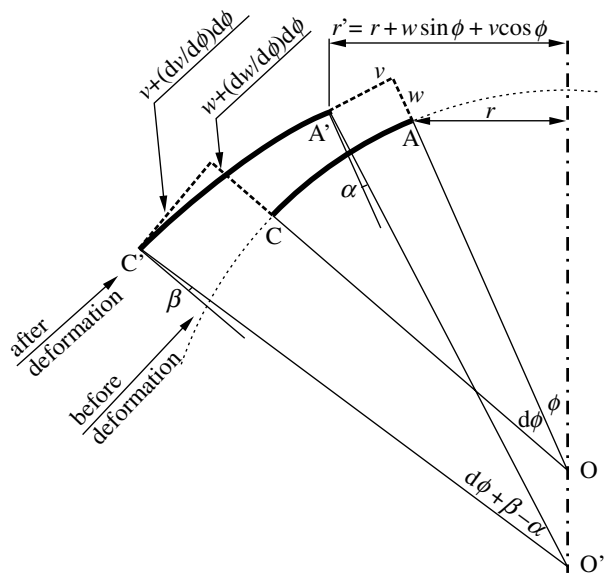

Figure 8. Displacements and rotations in the Y–Z plane.

circles as shown in figure 6. The element is assumed to have both bending and axial stiffness. It is analysed under a uniform IOP, p, acting in the negative local Z-direction (for background reading see Timoshenko & Woinowsky-Krieger (1959) and Gibson (1980)).

Force equilibrium in the Y-direction (also called the meridian direction) yields

$$\frac{\mathrm{d}(N_\varphi r\,\mathrm{d}\theta)}{\mathrm{d}\varphi}\,\mathrm{d}\varphi - N_\theta R\,\mathrm{d}\varphi\,\mathrm{d}\theta\cos\varphi - Q_\varphi r\,\mathrm{d}\theta\,\mathrm{d}\varphi = 0 \tag{5.1}$$

or

$$\frac{\mathrm{d}(N_\varphi r)}{\mathrm{d}\varphi} - N_\theta R\cos\varphi - Q_\varphi r = 0, \tag{5.2}$$

where $r = R\sin\varphi$ and R is the radius of the corneal median surface, see figure 7. Similarly, force equilibrium in the Z-direction yields

$$\frac{\mathrm{d}(Q_\varphi r\,\mathrm{d}\theta)}{\mathrm{d}\varphi}\mathrm{d}\varphi + N_\theta R\,\mathrm{d}\varphi\,\mathrm{d}\theta\sin\varphi + N_\varphi r\,\mathrm{d}\theta\,\mathrm{d}\varphi - pR\,\mathrm{d}\varphi\,r\,\mathrm{d}\theta = 0 \tag{5.3}$$

or

$$\frac{\mathrm{d}(Q_\varphi r)}{\mathrm{d}\varphi} + N_\theta R\sin\varphi + N_\varphi r - pRr = 0. \tag{5.4}$$

Finally, moment equilibrium about the X-axis gives

$$\frac{\mathrm{d}(M_\varphi r\,\mathrm{d}\theta)}{\mathrm{d}\varphi}\,\mathrm{d}\varphi - Q_\varphi r\,\mathrm{d}\theta\,(R\,\mathrm{d}\varphi) - M_\theta(R\,\mathrm{d}\varphi)\,\mathrm{d}\theta\cos\varphi = 0 \tag{5.5}$$

or

$$\frac{\mathrm{d}(M_\varphi r)}{\mathrm{d}\varphi} - Q_\varphi rR - M_\theta R\cos\varphi = 0. \tag{5.6}$$

Equations (5.2), (5.4) and (5.6) are not enough to determine the values of the five unknowns N_θ, N_φ, Q_φ, M_θ and M_φ. More equations are needed and these can be obtained by considering the deformed shape of the element ABCD in figure 8. Study of this figure reveals that

$$\varepsilon_\varphi = \frac{\mathrm{A'C'} - \mathrm{AC}}{\mathrm{AC}} = \frac{(\mathrm{d}v/\mathrm{d}\varphi)\,\mathrm{d}\varphi + (R+w)\,\mathrm{d}\varphi - R\,\mathrm{d}\varphi}{R\,\mathrm{d}\varphi} = \frac{\mathrm{d}v}{R\,\mathrm{d}\varphi} + \frac{w}{R}, \tag{5.7}$$

$$\varepsilon_\theta = \frac{2\pi r' - 2\pi r}{2\pi r} = \frac{2\pi(r + w\sin\varphi + v\cos\varphi) - 2\pi r}{2\pi r} = \frac{w\sin\varphi + v\cos\varphi}{r} = \frac{w + v\cot\varphi}{R}, \tag{5.8}$$

where $r = R\sin\varphi$.

Now, with the rotation of the element, the centre point O will move to O′ resulting in a change in the central angle from $\mathrm{d}\varphi$ to $\mathrm{d}\varphi + \beta - \alpha$. Therefore, while length AC is $R\,\mathrm{d}\varphi$, the length of the deformed arc A′C′ will be $R'(\mathrm{d}\varphi + \beta - \alpha)$. The change in curvature in the meridian direction can then be determined as

$$\chi_\varphi = \frac{1}{R'} - \frac{1}{R} = \frac{(\mathrm{d}\varphi + \beta - \alpha)}{\mathrm{A'C'}} - \frac{\mathrm{d}\varphi}{\mathrm{AC}}.$$

Substituting values for AC and A′C′ from equation (5.7), χ_φ is obtained as

$$\chi_\varphi \cong \frac{-1}{R^2}\left(w + \frac{\mathrm{d}v}{\mathrm{d}\varphi}\right). \tag{5.9}$$

Similarly, by considering the deformation in the parallel direction, the corresponding change in curvature, χ_θ, is obtained as

$$\chi_\theta \cong \frac{\cot\varphi}{R^2}\left(v + \frac{\mathrm{d}w}{\mathrm{d}\varphi}\right). \tag{5.10}$$

5.1. Overall equations

The meridian and parallel strains, ε_φ and ε_θ, can be related to N_φ and N_θ according to Hooke's Law,

$$\varepsilon_\varphi = \frac{1}{Et}(N_\varphi - \nu N_\theta), \tag{5.11}$$

$$\varepsilon_\theta = \frac{1}{Et}(N_\theta - \nu N_\varphi), \tag{5.12}$$

where E is the material's modulus of elasticity and ν is Poisson's ratio. Poisson's ratio is taken as 0.5 based on the assumption that the cornea behaves as an incompressible body (Bryant & McDonnell 1996). Therefore,

$$\left.\begin{aligned} N_\varphi &= \frac{Et}{(1-\nu^2)}(\varepsilon_\varphi + \nu\varepsilon_\theta), \\ N_\theta &= \frac{Et}{(1-\nu^2)}(\varepsilon_\theta + \nu\varepsilon_\varphi). \end{aligned}\right\} \tag{5.13}$$

Furthermore, M_φ and M_θ can be related to the changes in curvature in the following form:

$$M_\varphi = -D(\chi_\varphi + \nu\chi_\theta) \quad \text{and} \quad M_\theta = -D(\chi_\theta + \nu\chi_\varphi), \tag{5.14}$$

where D is the flexural rigidity per unit width of the corneal surface which is equal to $Et^3/12(1-\nu^2)$.

The values of ε_φ, ε_θ, χ_φ and χ_θ in terms of v and w as given in equations (5.7)–(5.10) can now be substituted into equations (5.13) and (5.14) to obtain four new equations that, together with equations (5.2), (5.4) and (5.6), give seven equations in the seven unknowns: N_φ, N_θ, Q_φ, M_φ, M_θ, v and w.

These equations have been solved for the case with a pinned edge to represent laboratory boundary conditions, where at $\varphi = \gamma$ (see figure 6*b*) both $M_\varphi = 0$ and the horizontal displacement equals zero. In this case,

$$N_\varphi = \frac{pR}{2}, \tag{5.15}$$

$$N_\theta = \frac{pR}{2} - \frac{pR}{2}(1-\nu)\mathrm{e}^{\beta\eta}(\cos\beta\eta), \tag{5.16}$$

$$M_\varphi = \frac{pR^2}{4\beta^2}(1-\nu)\mathrm{e}^{\beta\eta}(\sin\beta\eta), \tag{5.17}$$

$$M_\theta = \nu M_\varphi, \tag{5.18}$$

Rise (w at $\varphi = 0$)

$$= \frac{pR^2}{2Et}(1-\nu) - \frac{\nu R}{Et}\frac{pR}{2}(1-\nu)\mathrm{e}^{-\beta\gamma}(\cos\beta\gamma), \tag{5.19}$$

where $\beta = (R/t)^{1/2}[3(1-\nu^2)]^{1/4}$ and $\eta = \varphi - \gamma$. Equations (5.15)–(5.19) can be simplified for the case where the bending stiffness of the cornea can be ignored and the cornea assumed to act as a membrane. In this case,

$$N_\theta = N_\varphi = \frac{pR}{2}, \quad M_\theta = M_\varphi = 0$$

and

$$\text{Rise} = \frac{pR^2}{2Et}(1-\nu).$$

5.2. Mathematical procedure

At the inflation point, the corneal height, H_0, and the diameter of the interface between the cornea and the sclera, S, are measured experimentally. The initial radius is determined from

$$R_0^2 = \left(\frac{S}{2}\right)^2 + (R_0 - H_0)^2. \tag{5.20}$$

After the first pressure application, p_1, the corneal height will increase by the apical rise recorded experimentally,

$$H_1 = H_0 + \text{Rise}_1, \tag{5.21}$$

and the corresponding radius is obtained from

$$R_1 = \left[\left(\frac{S}{2}\right)^2 + (R_1 - H_1)^2\right]^{1/2}. \tag{5.22}$$

Assuming no change in volume of material in the cornea after loading,

$$2\pi R_0 H_0 t_0 = 2\pi R_1 H_1 t_1. \tag{5.23}$$

Therefore, the new thickness, t_1, is

$$t_1 = \frac{R_0 H_0 t_0}{R_1 H_1}. \tag{5.24}$$

Also angle γ becomes

$$\gamma_1 = \sin^{-1}\left(\frac{S}{2R_1}\right). \tag{5.25}$$

The values of R_1, p_1, t_1 and γ_1 are then substituted into equation (5.19) to obtain a value for the current modulus of elasticity, E_1. The corresponding strain, ε_1, can be determined using equation (5.11) after obtaining values for N_φ and N_θ from equations (5.15) and (5.16), respectively. The corresponding stress is also determined from

$$\sigma_1 = \varepsilon_1 E_1. \tag{5.26}$$

This process is repeated for every pressure increment and the experimental values of the pressure and rise are used, as explained, to obtain the corresponding values of stress and strain. The results for each of the 20 tests were analysed and the average stress–strain curve obtained is shown in figure 9.

6. NUMERICAL MODELLING

Numerical modelling based on the finite-element method is used to accurately predict the performance of porcine corneas and to provide a detailed account of their response to various mechanical actions. Previous studies attempted this approach with varying degrees of success. Buzard (1992) and Bryant & McDonnell (1996) developed a finite-element model in which corneas were modelled using two-dimensional axisymmetric elements. Their work confirmed the effectiveness of numerical modelling in corneal biomechanics, but was unable to model asymmetrical effects such as disease or injury. A more detailed three-dimensional model was

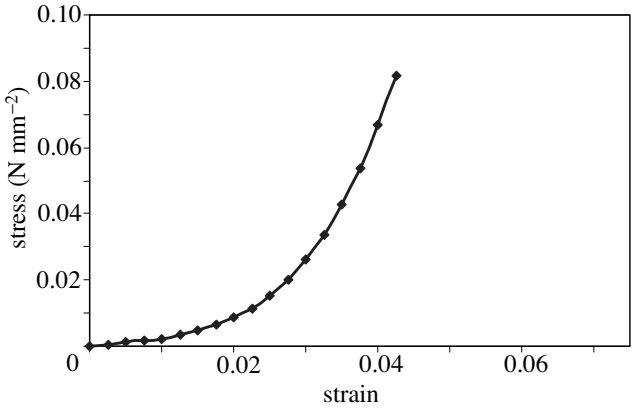

Figure 9. The average stress–strain relationship obtained from the trephinate inflation tests.

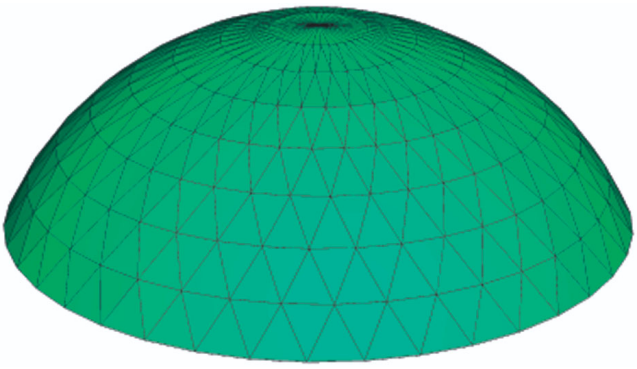

Figure 10. Three-dimensional numerical model.

used by Pinsky & Datye (1991) to predict the immediate change in corneal topography following refractive surgery. This model was based on a linear elastic behaviour pattern, despite the strong evidence confirming the visco-elastic, nonlinear material behaviour. Similar assumptions were adopted by Velinsky & Bryant (1992), who produced a structural model of the whole eye to determine the number and depth of cuts in surgical operations to correct myopia. Their work showed how finite-element modelling could be customized so that the process becomes patient specific using clinically measured data.

The numerical models developed in this research attempt to improve accuracy by using:

(1) the corneal topography data determined experimentally;
(2) the material constitutive relationship obtained from the trephinate inflation tests; and
(3) a three-dimensional modelling strategy able to represent unsymmetrical effects, see figure 10.

The models are comprised of triangular thin shell elements with six degrees of freedom per node $(u, v, w, \theta_x, \theta_y, \theta_z)$. The Abaqus software package (Hibbitt, Karlsson and Sorenson, Inc. 2001), known for its reliability and versatility, is used in this work. The nonlinear material stress–strain property is incorporated using a hyperelastic material model available in Abaqus based on Ogden's strain energy function (Ogden 1984):

$$U = \sum_{i=1}^{N} \frac{2u_i}{\alpha_i^2}(\lambda_1^{\alpha i} + \lambda_2^{\alpha i} + \lambda_3^{\alpha i} - 3) + \sum_{i=1}^{N} \frac{1}{D_1}(J^{\mathrm{el}} - 1)^{2i}, \tag{6.1}$$

where λ_i are the principal stretches, N is a material parameter, J^{el} is the elastic volume ratio and u_i, α_i and D_i are temperature-dependent material parameters.

The complexity of the structure and the form of the cornea at both the micro and macro levels presented a particular challenge during the development of the models. On the one hand, there was a desire to simulate the real structure and form of the cornea in order to improve accuracy and, on the other, there was a practical requirement to simplify the models and keep them at a reasonable level of complexity to reduce cost. In order to strike the best balance between cost and accuracy, a study was conducted to identify the effect of individual parameters on the models' accuracy. The parameters that were found to have a small or a negligible effect (with an effect on accuracy below 2%) were not considered in the final construction of the model.

The study considered several parameters, including the density of the finite-element mesh, the thickness variation between the corneal centre and edge, the composite structure of the cornea, the significance of the out-of-plane flexural and torsional resistance of the cornea and the boundary condition along the edge of the cornea as provided by the sclera. The accuracy of the model in each case was checked against the pressure–apical rise results of the trephinate tests. The following discussion considers the effect of these parameters one by one.

6.1. Density of finite-element mesh

Increasing the density of finite-element meshes normally has two effects: (1) better accuracy; and (2) higher analysis cost due to the larger number of nodes and hence number of equilibrium equations. The trend of improved accuracy with denser meshes commonly continues up to a certain limit, beyond which the benefit of using denser meshes diminishes. The study presented in this section is intended to determine this limit.

Figure 11 shows the pressure–apical rise predictions for a typical trephinate specimen tested under increasing pressure in the present experimental programme. The predictions are obtained using numerical models employing 320, 640 and 960 triangular elements. The models have between 8 and 12 rings of elements and between 40 and 80 elements per ring. The figure shows that the accuracy of predictions is not improved with meshes using more than 640 elements. Increasing the mesh density from 640 to 960 elements results in only 0.80% improvement in accuracy and would therefore be difficult to justify considering the associated increase in analysis cost. This could be compared with the 3.5% improvement in accuracy when using 640 rather than 320 elements.

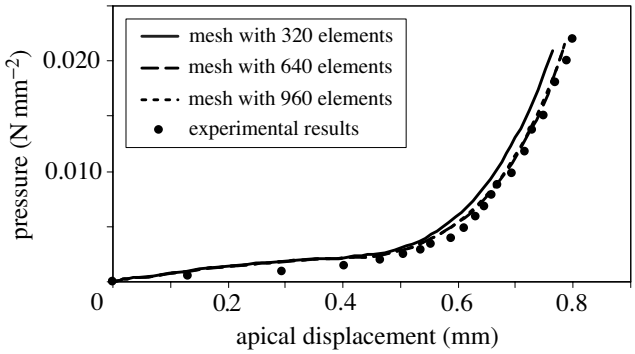

Figure 11. Effect of using finite-element meshes with different element densities.

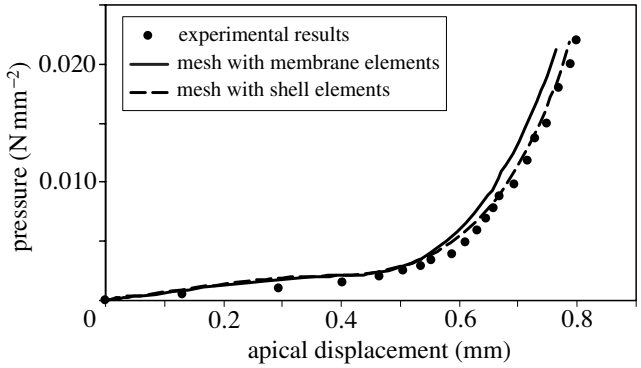

Figure 12. Effect of using finite-element meshes with shell and membrane elements.

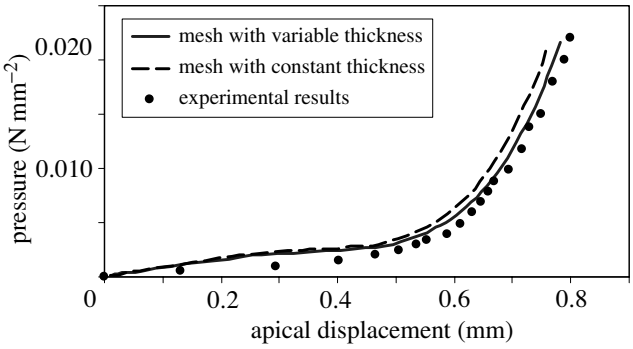

Figure 13. Effect of using finite-element meshes with constant and variable corneal thickness.

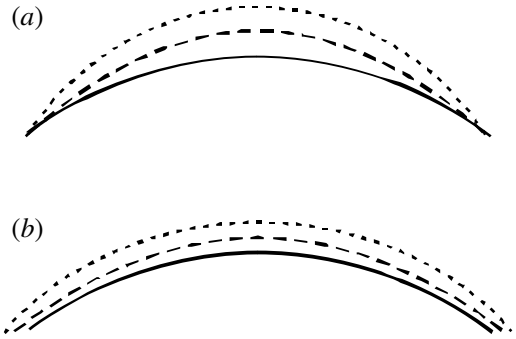

Figure 14. Deformation of the cornea under IOP while ignoring or assuming scleral deformation: (*a*) without scleral deformation; (*b*) with scleral deformation.

6.2. Bending resistance of cornea

Two options are available in modelling the cornea. It could be modelled using shell elements considering both in-plane and out-of-plane effects (and even the composite nature of the cornea) or modelled with membrane elements that ignore the corneal flexural and torsional out-of-plane resistance. The second option is undoubtedly cheaper in analysis cost.

Both options have been attempted when modelling the behaviour of a typical experimental trephinate specimen and the predictions are presented in figure 12. Comparison of the results against experimental data clearly confirms the significance of the out-of-plane effects. Using membrane elements in this example leads to an average loss in accuracy of 4.3% as compared to the model with shell elements.

6.3. Thickness variation

The corneal thickness is smallest at the centre and grows gradually towards the limbus—the intersection with the sclera. In modelling terms, it is easier to assume a constant thickness than to consider the actual thickness variation. The effect of this simplification on the modelling accuracy is illustrated using the example shown in figure 13. In this figure, the predictions using a model with a variable thickness (0.645 mm along the edge and 0.545 mm at the centre) and a model with a constant thickness (0.595 mm, which is the average between the corneal central and edge thickness) are plotted against the experimental results. The results show only a small change in predictions caused by this simplification. Assuming a constant thickness results in an average change in predictions of 2%. This outcome, which was repeated for other trephinate tests, indicates that this modelling simplification could be adopted without a significant loss in accuracy.

6.4. Corneo–scleral connection

A whole-eye model incorporating both the cornea and the sclera, and the enclosed fluid, would undoubtedly provide a better representation of the actual state of the cornea, including the boundary conditions along its edge, than a model of the cornea alone. However, a whole-eye model is clearly more expensive to develop and run. A compromise could be reached if the cornea-only model could be formed such that the boundary conditions along its edge are accurately represented. This can be done whilst appreciating that the sclera, although stiffer than the cornea, should not be expected to provide the cornea with supports that are prevented from both translation and rotation. In reality, the sclera will deform under pressure or other effects and this deformation will affect the corneal behaviour, see figure 14.

A study has been carried out to find a reasonable approximation of the corneal edge supports. The first

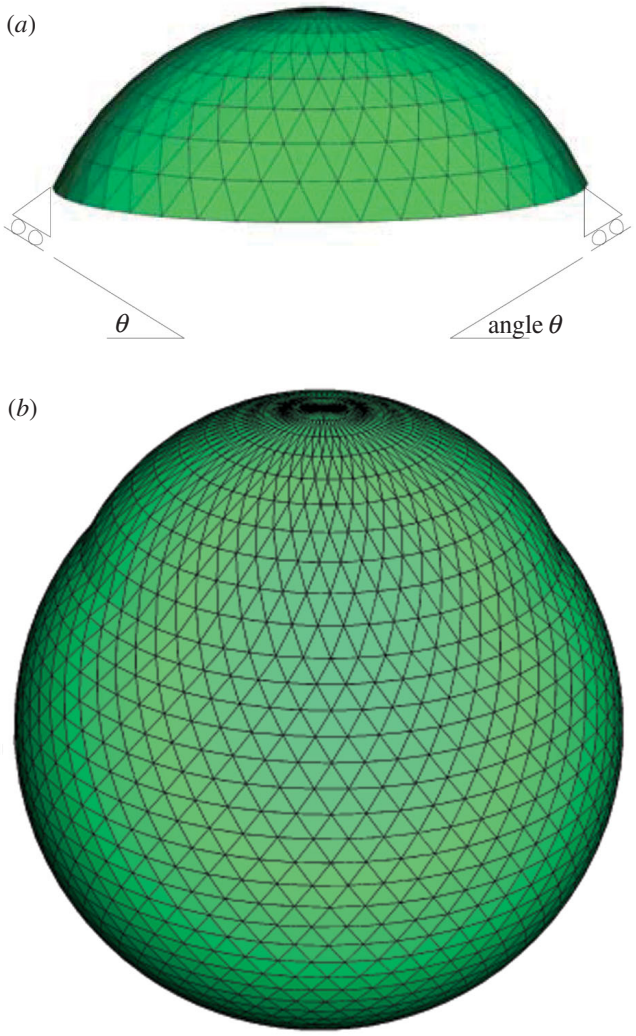

Figure 15. Numerical models: (*a*) corneal model with edge roller supports, the angle θ changed in the study between 35° and 45°; (*b*) full ocular model.

approach considers the edge nodes of the corneal model to be attached to roller supports in an inclined direction as shown in figure 15. The angle of support orientation, θ, is changed between 30° and 60°, and the predictions of the model with different support orientations are presented in figure 16, where they are compared with the results of a whole-eye model. It is evident that a support orientation of 40° provides the best match with the whole-eye model with an average difference of 0.7%. This approach is similar to that adopted by Orssengo & Pye (1999).

With these inclined supports, the cornea-only model would be expected to approximate the whole-eye model and be suitable for applications where the focus is only on the corneal behaviour. Applications that involve the sclera or require the modelling of the internal eye fluid would still need a whole-eye model. Examples include the modelling of dynamic tonometry, where the eye is subjected to an air impulse in a procedure used to measure the IOP. In this case, the pressure waves inside the eye and the fluid structure interaction during the movement of the pressure waves must be

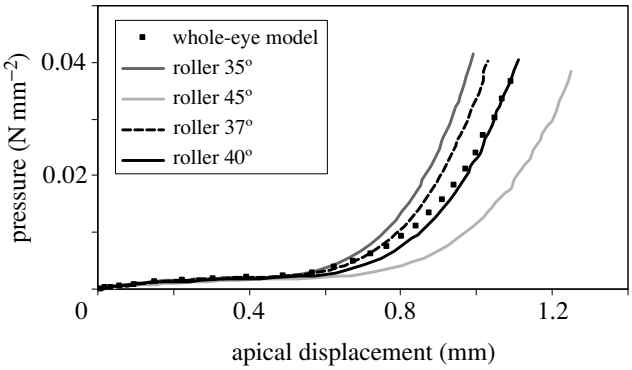

Figure 16. Comparison between the cornea model with different support orientations and the whole-eye model.

considered. For these applications, a whole-eye model must be used. Further work will be undertaken to study other approximations of the corneo–scleral connection, for instance using a roller support with a rotational spring. This idealization would be expected to provide a more accurate representation of the effect of the sclera in resisting corneal curvature.

7. RESULTS OF THE NUMERICAL MODEL

7.1. Further insight into experimental behaviour

The numerical model has been used to describe the performance of the trephinate specimens tested in this research to a level of detail impossible to achieve with laboratory tests. The information obtained includes the distributions of displacement, stress and strain over the surface area of the cornea. Examples of the output of the model for a typical trephinate specimen under IOP = 2 kPa or 15.04 mmHg are given in figure 17. Based on the initial study to identify the parameters with significant influence, the model has 640 shell elements and constant thickness. It has pinned supports along the edge nodes to simulate the laboratory test conditions (note that in this case the sclera did not form part of the test specimens). The model also incorporates the nonlinear material constitutive relationship obtained from the trephinate inflation tests and implemented using the hyperelastic material model available in Abaqus. The load–apical rise results match the laboratory data closely, as shown in figure 17. In addition to these results, the deformation, stress and strain distributions given in the figure provide a useful insight into the behaviour of the corneal specimen and the changes encountered due to elevated IOP.

7.2. Practical applications

7.2.1. Modelling of keratoconic eyes. Keratoconus is characterized by a deterioration of the structure of the cornea mainly in the form of a localized loss of up to 75% of the corneal tissue (Bron 1988). As a result, the cornea changes shape under IOP, with serious implications on its refractive power (Andreassen 1980; Edmund 1989). The disease affects 55 individuals per 100 000 of the general population. Research is currently underway to

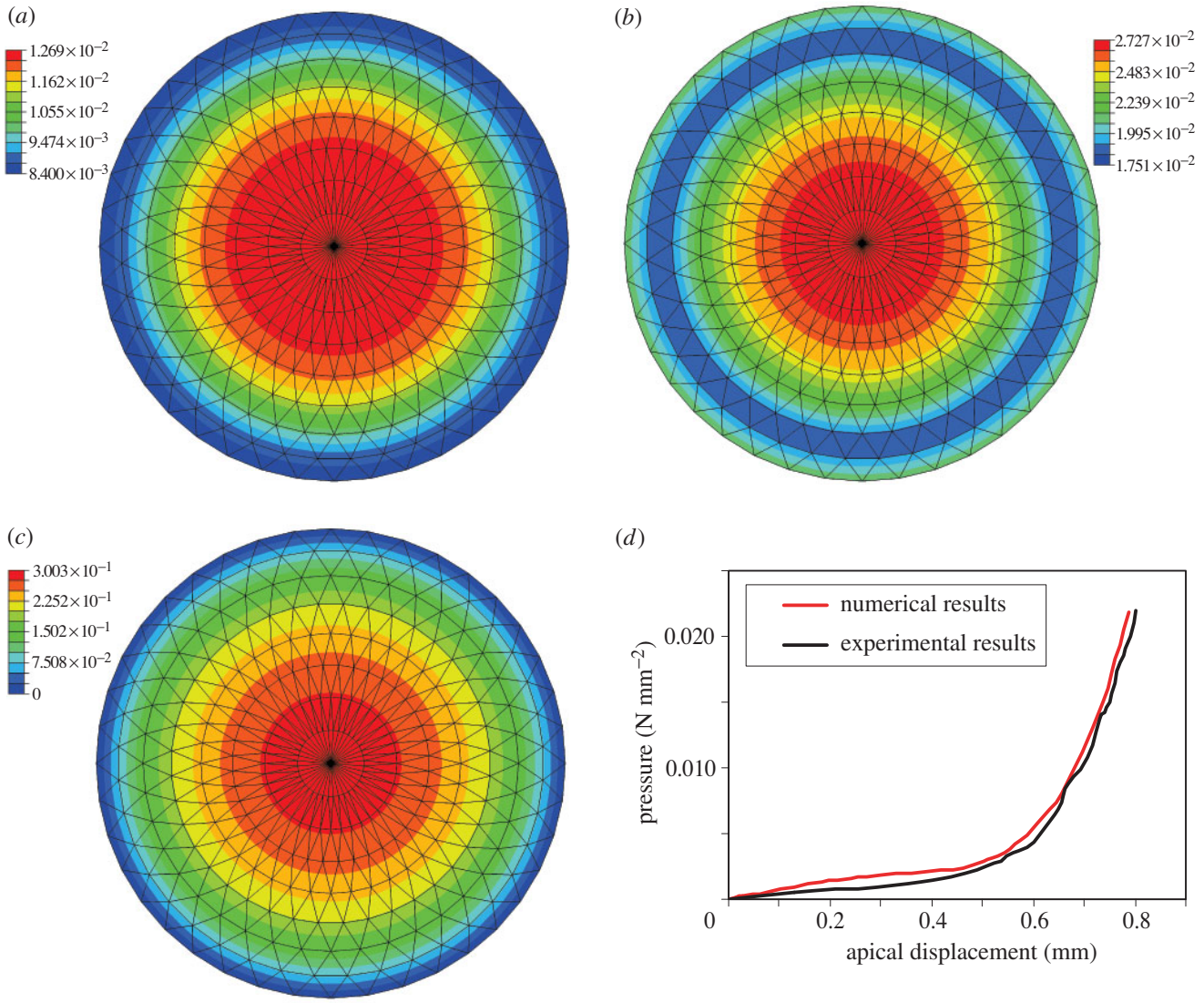

Figure 17. Example results of the numerical model under an IOP of 2 kPa (15.04 mmHg): (*a*) distribution of Mises strain (N mm^{-2}); (*b*) distribution of maximum principal strain (N mm^{-2}); (*c*) distribution of displacement (mm); (*d*) comparison between numerical and experimental IOP rise results.

study the effect of tissue loss on the corneal topography and hence refractive power. The research assumes the disease can affect the cornea either at or away from its centre. The thickness loss and the percentage of the surface area affected by the disease are two more parameters in the study.

The study is based on using the numerical model to simulate the effects of keratoconus on the corneal biomechanics. In particular, predictions of deformation, change of shape and stress distribution are important, as they may present useful information for the clinical management of the disease. Typical examples of the results obtained from the initial parts of this work are presented in figure 18 for two cases with keratoconus affecting the centre of the cornea and an area half-way between the centre and the edge. A maximum tissue loss of 75% of the average thickness is assumed at the centre of the disease, gradually reducing to no loss at the edge of the affected area. The affected area is assumed to have a diameter equal to a quarter of the corneal meridian length. The predicted behaviour for a normal cornea is also shown in figure 18 for comparison.

The results presented in figure 18 show the increased corneal deformation as a result of the disease. This analysis suggests an increase in the elevation of the cornea of approximately 0.080 mm, which may have a significant effect on the refractive power of the eye, although this may be partially countered by accommodation causing changes to the lens and the shape of the cornea (He *et al.* 2003). The distribution of the deformation is dependent on the location of the affected area; when the tissue loss is at the centre, the deformation distribution remains symmetrical, but the symmetry is lost when the affected area is shifted away from the centre. This type of approach can help provide insights into the cause of this disease, the effects of loss of tissue and corneal stiffness and the progression of the disease. Further comparison with patient specific data will provide calibration and validation of the computer models.

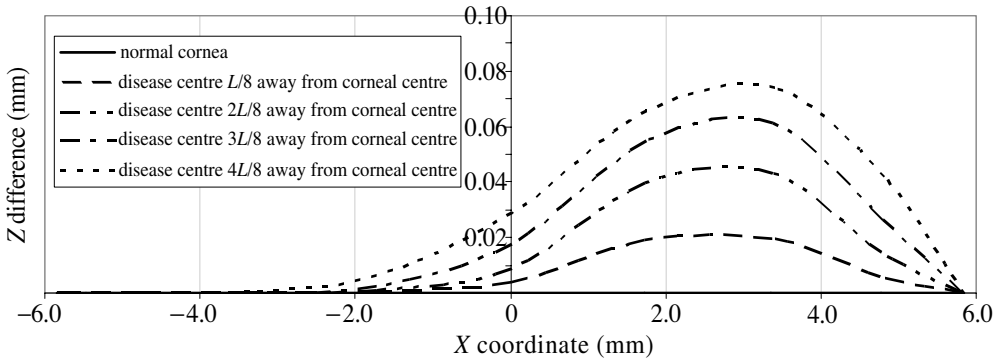

Figure 18. Effect of keratoconus on the corneal profile under an IOP of 2 kPa; L is the meridian length of the cornea.

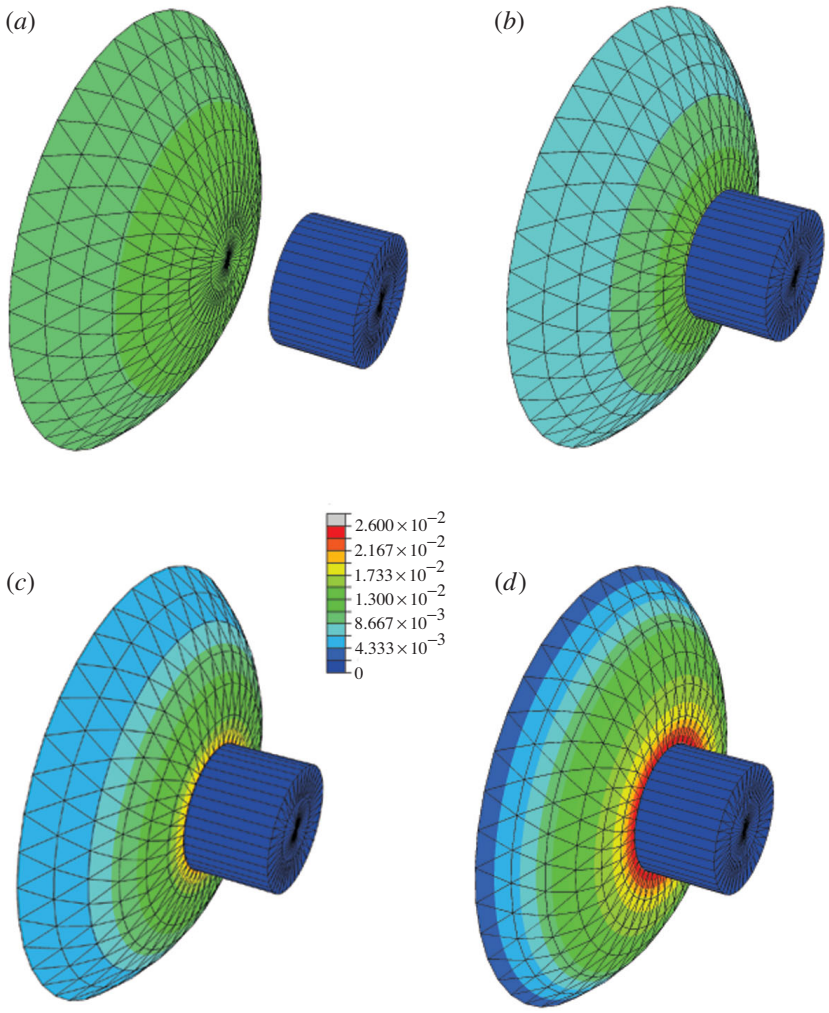

Figure 19. Modelling the GAT procedure using a cornea-only model (units are N mm^{-2}): (a) before contact; (b) initial contact; (c) intermediate step; (d) full applanation.

7.2.2. Static tonometry. Tonometry is a procedure to measure IOP of the eye. Ophthalmologists use the IOP measurements to diagnose a number of conditions including hyphema (trauma and inflation of the iris) and glaucoma, the second most common cause of irreversible blindness in the world (Wilson & Kass 2002). The two common tonometry techniques are the Goldmann applanation tonometer (GAT) and the pneumo-tonometer. The GAT is based on making a pseudo-static measurement of the force required to flatten a fixed central area of the cornea with 3.06 mm diameter (Goldmann & Schmidt 1961; Feltgen *et al.* 2001; Whitacre *et al.* 1993), while the pneumo-tonometer is a dynamic test where the eye is subjected

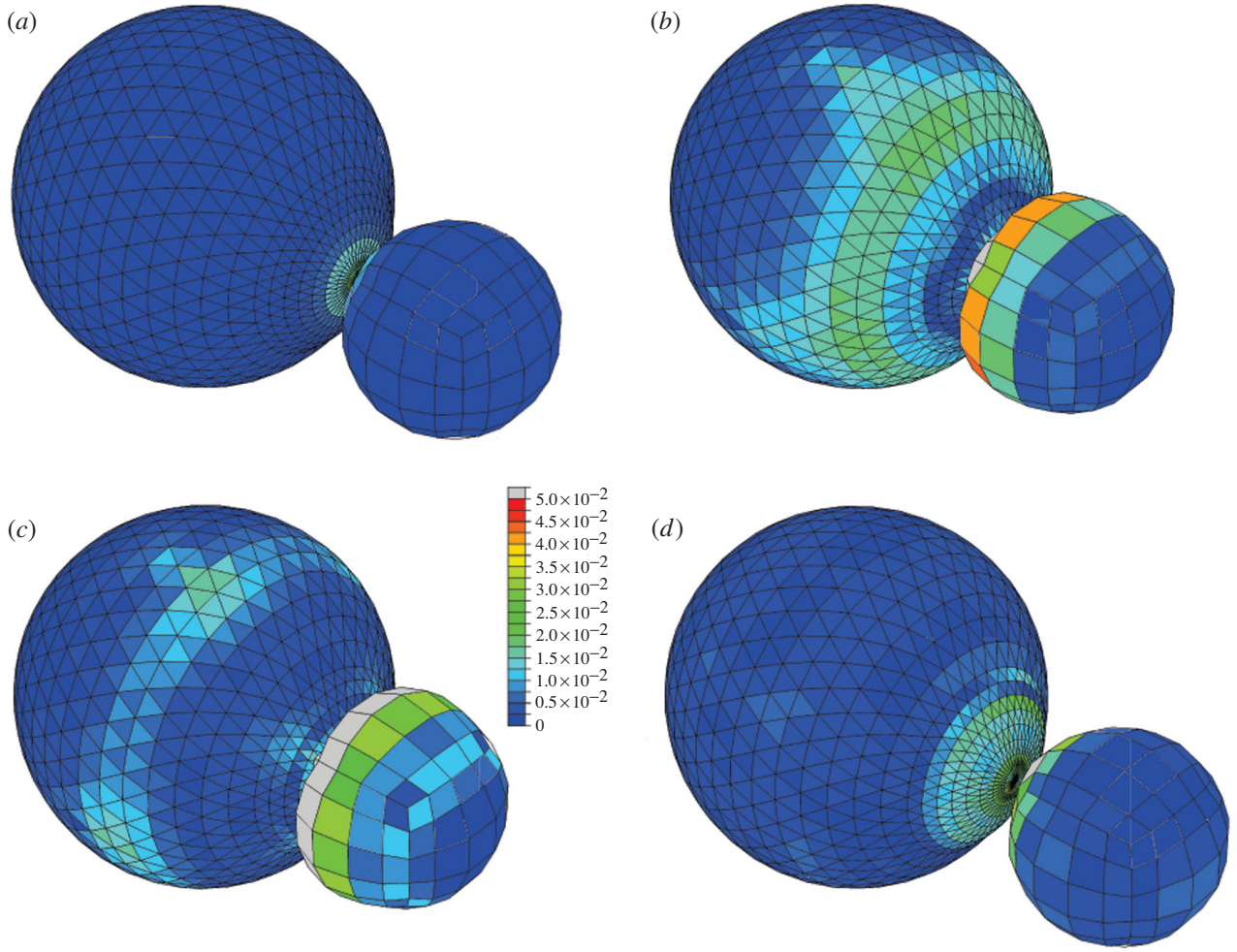

Figure 20. The pressure wave travelling through the eye in dynamic tonometry (units are $\mathrm{N\,mm^{-2}}$): (*a*) initial contact; (*b*) pressure wave; (*c*) dispersion of pressure wave; (*d*) pressure wave back at cornea following impact.

to an air impulse and the time taken to flatten the central cornea is used to determine the value of the IOP.

A study is underway to numerically model the GAT procedure with the view of determining the effect of corneal parameters such as thickness and diameter on the IOP measurements. The study is parametric and involves corneal models with different dimensions and IOPs. The corneas are subjected to a static pressure from a solid object with 3.06 mm diameter representing the GAT. The pressure required to achieve complete contact between the tonometer and the cornea is measured and plotted to enable a comparison of the outcome of the procedure with the actual IOP in the eye.

The model used in this study is a cornea-only model, as the connection with the sclera and the interaction between the eye and its internal fluid is expected to have little effect on the results. The cornea model has 640 shell elements and is provided with roller supports (with 40° inclination) along all edge nodes. The modulus of elasticity and Poisson's ratio are taken as $0.0229 \times \mathrm{IOP}$ and 0.5, respectively, according to Orssengo & Pye (1999). The tonometer is modelled using 40 five-sided solid elements with two triangular and three rectangular faces as shown in figure 19. The figure shows the progress of the procedure until complete contact is established. The initial parts of the study have compared the results of fully explicit models of the indentor with simulations, where the indentor has been represented by a uniformly distributed load (as has been done previously, Orssengo & Pye (1999)), for both linear and nonlinear elastic corneal models. Further comparisons have been made with clinical data from Doughty & Zaman (2000). Both data sets indicate that the IOP is over-predicted for thin corneas and under-predicted for thick corneas. Finite-element analysis shows a strong correlation with the clinical studies and the prediction using explicit modelling of the indentor and material nonlinearity produces the best results. Further work will help provide more accurate correction factors for IOP measurements to accommodate varying corneal thickness.

7.2.3. Dynamic tonometry. A similar study is being carried out to determine the effect of corneal thickness and diameter on the IOP measurements using the pneumo-tonometer. This procedure is based on measuring the time taken for an air impulse to flatten

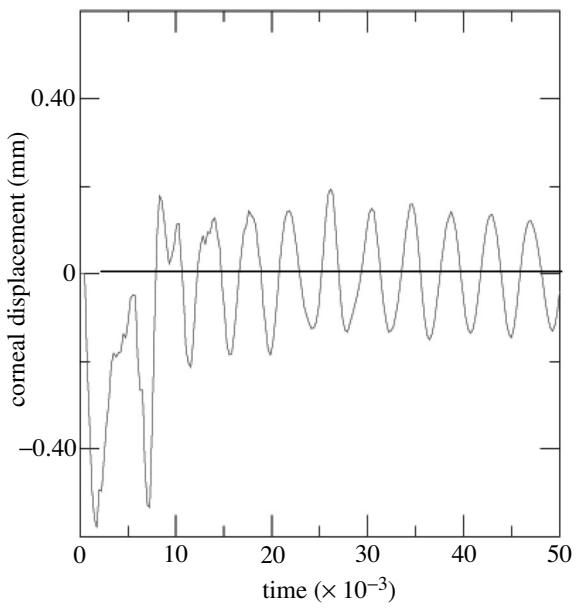

Figure 21. The displacement at the corneal centre point upon impact with the air impulse in pneumo-tonometry.

the central region of the cornea. As this procedure is a non-contact procedure and is quick to apply, it is currently finding increasing acceptance.

Pneumo-tonometry is a dynamic procedure and the interaction between the cornea and the sclera and between the eye and its internal fluid is certainly important for the accurate modelling of the procedure. A whole-eye model is used in this study with the cornea and sclera modelled using 640 and 3200 shell elements, respectively, see figure 20. The internal fluid is modelled as a set of 3840 internal fluid elements with the initial pressure being equal to the eye's IOP. The air impulse is modelled as a spherical formation of 150 four-sided membrane elements enclosing 150 fluid elements with density and pressure equal to the air density and atmospheric pressure, respectively. The air impulse model is triggered with an initial velocity towards the centre of the cornea. The displacements of the cornea upon impact at several points at and away from the centre are monitored and plotted to enable the determination of the time needed to flatten the central corneal region. The flow of pressure waves within the eye, as seen in figure 20, is monitored along with the associated pressure changes at the region of impact, to improve the understanding of the behaviour of the eye structure and to enable more accurate correction factors for the IOP measurements to be obtained.

The dynamic response of the eye to the impact with the air impulse is illustrated in figure 21, showing the displacement of the corneal centre point with time. A phenomenon that has been observed experimentally and confirmed in this study is how the cornea deforms in only the posterior direction in the first two deformation cycles. This finding is currently under study to establish the reasons behind it. The possibilities include the interaction between the eye and its internal fluid and the peculiar geometry of the corneo–scleral structure.

8. CONCLUSIONS

The research presented in this paper is part of a long-term project to develop accurate predictive tools that can assist in the clinical management of the cornea. Accuracy is achieved through the use of laboratory tests that are representative of *in vivo* conditions and the adoption of realistic corneal topography and material constitutive relationships. Laboratory inflation tests of corneal trephinates confirm the highly nonlinear behaviour of the material. Mathematical analyses are performed to determine the material constitutive relationship and they confirm that the nonlinear behaviour observed experimentally is primarily due to the nature of the material and its microstructure. An assumption of a linear material behaviour might simplify the analysis, but will undoubtedly lead to serious underestimations of stiffness under high pressures.

Enhancements of the predictive models are underway to consider the hysteretic behaviour observed under cyclic loading and to improve the stability of analysis at the stage where the modulus of elasticity increases rapidly. Planned applications of the model include predicting the effects of sports injuries and refractive surgery. Research is also underway to study the loading conditions in tonometry with a view to improving the accuracy of existing techniques in measuring the IOP.

This research demonstrates the usefulness of engineering analytical tools within multi-disciplinary projects in the field of biomechanics.

This work was partially supported by a Doctorate Training award from the Engineering and Physical Sciences Research Council. The authors are grateful for the valuable contributions made by Mr David Garway-Heath, the lead clinical researcher of the Glaucoma Research Unit, Moorefields Hospital, London.

REFERENCES

Andreassen, T. T., Simonsen, A. H. & Oxlund, H. 1980 Biomechanical properties of keratoconus and normal corneas. *Exp. Eye Res.* **31**, 435–441.

Bron, A. J. 1988 Keratoconus. *Cornea* **7**(3), 163–169.

Bryant, M. R. & McDonnell, P. J. 1996 Constitutive laws for bio-mechanical modelling of refractive surgery. *J. Bio-Mech. Eng.* **118**, 473–481.

Buzard, K. A. 1992 Introduction to bio-mechanics of the cornea. *Refractive Corneal Surgery* **8**, 127–138.

Doughty, M. J. & Zaman, M. L. 2000 Human corneal thickness and its impact on intraocular pressure measures: a review and meta-analysis approach. *Surv. Ophthalmol.* **44**, 367–408.

Edmund, C. 1989 Corneal topography and elasticity in normal and keratoconic eyes. *Acta Ophthalmol.* **67**(193).

Feltgen, N., Leifert, D. & Funk, J. 2001 Correlation between central corneal thickness, applanation tonometry, and direct intracameral IOP readings. *Br. J. Ophthalmol.* **85**, 85–87.

Gibson, J. E. 1980 *Thin shells: computing and theory.* Oxford: Pergamon.

Goldmann, H. & Schmidt, T. 1961 Uber Applanations-tonometrie. *Ophthalmologica* **134**, 221.

He, J., Gwiazda, J., Thorn, F., Held, R. & Huang, W. 2003 Change in corneal shape and corneal wave-front aberrations with accommodation. *J. Vision.* **3**, 456–463.

Hibbitt, Karlsson and Sorensen, Inc. 2001 *Abaqus: standard user's manual*. Detroit, USA.

Hjortdal, J. O. 1993 Regional elastic performance of the human cornea. *J. Biomechanics* **29**(7), 931–942.

Hjortdal, J. O. 1998 On the biomechanical properties of the cornea with particular reference to refractive surgery. *Ophthalmol. J. Nordic Countries* **76**(225), 1–23.

Leibowitz, H. M. & Waring, G. O. 1998 *Corneal disorders: clinical diagnosis and management*, 2nd edn. New York: Saunders.

Nyquist, G. W. 1968 Rheology of the cornea: experimental techniques and results. *Exp. Eye Res.* **7**, 183–188.

Ogden, R. H. 1984 *Non-linear elastic deformations*. London: Prentice-Hall.

Orssengo, G. J. & Pye, D. C. 1999 Determination of the true intraocular pressure and modulus of elasticity of the human cornea in vivo. *Bull. Math. Biol.* **61**, 551–572.

Pinsky, P. M. & Datye, D. V. 1991 A microstructurally based finite element model of the incised human cornea. *Biomechanics* **24**(10), 907–922.

Radner, W., Zehetmayer, M., Aufreiter, R. & Mallinger, R. 1998 Interlacing and cross-angle distribution of collagen lamellae in the human cornea. *Cornea* **17**(5), 537–543.

Scott, J. E. 1991 Proteoglycan: collagen interactions and corneal ultrastructure. *Biochem. Eye—Biochem. Soc. Trans.* **19**, 877–881.

Timoshenko, S. & Woinowsky-Krieger, S. 1959 *Theory of plates and shells*. Tokyo: McGraw-Hill.

Velinsky, S. A. & Bryant, M. R. 1992 On the computer-aided and optimal design of keratorefractive surgery. *Refractive Corneal Surgery* **8**, 173–182.

Vito, R., Shin, T. & McCarey, B. 1989 A mechanical model of the cornea: the effects of physiological and surgical factors on radial kertotomy surgery. *Refractive Corneal Surgery* **5**, 82–87.

Whitacre, M. M., Stein, R. A. & Hassanein, K. 1993 The effect of corneal thickness on applanation tonometry. *Am. J. Ophthalmol.* **115**, 592–596.

Wilson, M. R. & Kass, M. A. 2002 The ocular hypertension treatment study: baseline factors that predict the onset of primary open-angle glaucoma. *Arch. Ophthalmol.* **120**, 714–720.

Woo, S. L. Y., Kobayashi, A. S., Schlegel, W. A. & Lawrence, C. 1972 Non-linear properties of intact cornea and sclera. *Exp. Eye Res.* **14**, 29–39.

Zeng, Y., Yang, J., Huang, K., Lee, Z. & Lee, X. 2001 A comparison of biomechanical properties between human and porcine cornea. *J. Biomechanics* **34**, 533–537.